Article

SOURCE DATA | TRANSPARENT PROCESS

EMBO reports

PI4-kinase and PfCDPK7 signaling regulate phospholipid biosynthesis in *Plasmodium falciparum*

Ranjana Maurya[1,†], Anuj Tripathi[1,†], Manish Kumar[1,2,3], Neelam Antil[2,4,5], Yoshiki Yamaryo-Botté[6], Praveen Kumar[1], Priyanka Bansal[1], Christian Doerig[7], Cyrille Y Botté[6,‡], T S Keshava Prasad[2,5,8,‡] & Pushkar Sharma[1,*,‡]

Abstract

PfCDPK7 is an atypical member of the calcium-dependent protein kinase (CDPK) family and is crucial for the development of *Plasmodium falciparum*. However, the mechanisms whereby PfCDPK7 regulates parasite development remain unknown. Here, we perform quantitative phosphoproteomics and phospholipid analysis and find that PfCDPK7 promotes phosphatidylcholine (PC) synthesis by regulating two key enzymes involved in PC synthesis, phosphoethanolamine-N-methyltransferase (PMT) and ethanolamine kinase (EK). In the absence of PfCDPK7, both enzymes are hypophosphorylated and PMT is degraded. We further find that PfCDPK7 interacts with 4'-phosphorylated phosphoinositides (PIPs) generated by PI4-kinase. Inhibition of PI4K activity disrupts the vesicular localization PfCDPK7. *P. falciparum* PI4-kinase, PfPI4K is a prominent drug target and one of its inhibitors, MMV39048, has reached Phase I clinical trials. Using this inhibitor, we demonstrate that PfPI4K controls phospholipid biosynthesis and may act in part by regulating PfCDPK7 localization and activity. These studies not only unravel a signaling pathway involving PfPI4K/4'-PIPs and PfCDPK7 but also provide novel insights into the mechanism of action of a promising series of candidate anti-malarial drugs.

Keywords CDPK; kinase; malaria; phospholipids; phosphoproteomics; signaling

Subject Categories Metabolism; Microbiology, Virology & Host Pathogen Interaction; Proteomics

DOI 10.15252/embr.202154022 | Received 20 September 2021 | Revised 30 October 2021 | Accepted 11 November 2021 | Published online 6 December 2021

EMBO Reports (2022) 23: e54022

Introduction

The malaria parasite *Plasmodium* spp is transmitted to the human host through the bite by an infected female *Anopheles* mosquito, which allows the entry of sporozoites into the bloodstream of the human host. The sporozoites then infect hepatocytes in the host liver to expand their population during an asymptomatic period of asexual schizogonic division, during which thousands of merozoites are formed. Merozoites enter the bloodstream and invade erythrocytes to initiate the intra-erythrocytic stages of parasite development, which gives rise to malaria pathogenesis. After the invasion of red blood cells (RBCs), the intracellular parasites mature from rings to trophozoites followed by asexual schizogonic division that results in the generation of ~30 merozoites per schizont within 48 h in the case of *P. falciparum*. Freshly egressed merozoites can infect fresh RBCs to start a new round of asexual division. Some parasites withdraw from proliferation and undergo sexual differentiation to male or female gametocytes, which can be ingested by the mosquito, in which sporogony occurs, resulting in the generation of infective sporozoites (Cowman *et al*, 2016).

CDPKs, a family of kinases that are restricted to plants and Alveolates (the taxon that includes Ciliates and Apicomplexa), are major effectors of calcium signaling in *Plasmodium* as well as the related apicomplexan parasite *Toxoplasma gondii,* and collectively regulate crucial processes, including host cell invasion, egress, growth, and sexual differentiation (Billker *et al*, 2004, 2009; Dvorin *et al*, 2010; Lourido *et al*, 2010; Sebastian *et al*, 2012; Gaji *et al*, 2014; Kumar *et al*, 2014, 2017; Morlon-Guyot *et al*, 2014; Treeck *et al*, 2014). Classical CDPKs contain a protein kinase domain and C-terminal calmodulin (CaM)-like domain, which are connected by a regulatory

1 Eukaryotic Gene Expression laboratory, National Institute of Immunology, New Delhi, India
2 Institute of Bioinformatics, International Tech Park, Bangalore, India
3 Manipal Academy of Higher Education, Manipal, India
4 ApicoLipid Team, Institute of Advanced Biosciences, CNRS UMR5309, Université Grenoble Alpes, INSERM U1209, Grenoble, France
5 Amrita School of Biotechnology, Amrita Vishwa Vidyapeetham, Kollam, India
6 Center for Systems Biology and Molecular Medicine, Yenepoya Research Centre, Yenepoya (Deemed to be University), Mangalore, India
7 NIMHANS IOB Proteomics and Bioinformatics Laboratory, Neurobiology Research Centre, National Institute of Mental Health and Neuro Sciences, Bangalore, India
8 School of Health and Biomedical Sciences, RMIT University, Bundoora, Vic., Australia
*Corresponding author. Tel: 91-11-26703791; Fax: 91-11-26742125; E-mail: pushkar@nii.ac.in
†These authors contributed equally to this work
‡These authors contributed equally to this work

Junction domain (Billker *et al*, 2009; Ahmed *et al*, 2012). The domain architecture of PfCDPK7 diverges from that of other members of the CDPK family. It has two N-terminal EF-hand calcium-binding motifs connected by a long linker to a PH-domain, with the kinase domain located at the C terminus (Kumar *et al*, 2014; Morlon-Guyot *et al*, 2014; Bansal *et al*, 2021). Despite the presence of the EF-hands, there is no experimental evidence of its regulation by calcium. This atypical kinase is conserved in *Toxoplasma* and *Plasmodium* and is able to interact with phosphoinositides PI4P and $PI(4,5)P_2$ via its PH domain (Kumar *et al*, 2014; Morlon-Guyot *et al*, 2014). Previously, we have demonstrated that the PH domain via which PfCDPK7 interacts with $PI(4,5)P_2$ is important for its localization to vesicular structures (Kumar *et al*, 2014). CDPK7 is critical for the development of both the rodent malaria parasite *P. berghei* and *P. falciparum*; it is indispensable for *P. berghei* (Tewari *et al*, 2010) and its knockout in *P. falciparum* is achievable (Solyakov *et al*, 2011) but severely impairs asexual parasite development (Kumar *et al*, 2014). Additional studies suggested that CDPK7 regulates the division of *P. falciparum* and *T. gondii* (Kumar *et al*, 2014; Morlon-Guyot *et al*, 2014) as well as the transition from ring to trophozoite during the *P. falciparum* erythrocytic cycle (Kumar *et al*, 2014).

The underlying mechanisms through which PfCDPK7 regulates parasite development remain unknown. In the present study, we have identified PfCDPK7-dependent molecular processes in *P. falciparum* blood stages. Quantitative phosphoproteomics of wild-type and PfCDPK7 knockout parasites revealed that the phosphorylation levels of proteins predicted to be involved in lipid metabolism and protein/lipid trafficking were significantly altered. Furthermore, we provide evidence that the biosynthesis of a major phospholipid, phosphatidylcholine (PC), is regulated by PfCDPK7. Finally, we show that the parasite's PI4-kinase PfPI4K regulates PfCDPK7 and is therefore also involved in PL biosynthesis.

Results

Identification of PfCDPK7-regulated pathways in *P. falciparum* asexual parasites by comparative phosphoproteomics

In order to elucidate the mechanism through which PfCDPK7 regulates the development of *P. falciparum*, we used a previously reported parasite line in which the *PfCDPK7* gene is disrupted by homologous recombination-dependent insertion. This line (PfCDPK7-KO) exhibits significant defects in parasite growth relative to the parental 3D7 clone, which is due to impaired ring to trophozoite maturation and division (Kumar *et al*, 2014). We performed quantitative phosphoproteomics on PfCDPK7-KO and wild-type 3D7 parasites to identify potential targets of PfCDPK7 signaling. Since PfCDPK7-KO parasites were defective in ring to trophozoite maturation, late ring–early trophozoites were used for this experiment (see Methods). iTRAQ-labeled peptides from PfCDPK7-KO and wild-type parasites were analyzed on high-resolution mass spectrometer. In all, 82 phosphosites from 68 proteins exhibited hypophosphorylation and 15 phosphosites from 13 proteins showed hyperphosphorylation in the PfCDPK7-KO parasites as compared to the wild-type (Dataset EV1). Fig 1A illustrates the number of phosphosites identified in the analysis and their respective fold-change in the mutant parasites. A subset of proteins that were found to be differentially phosphorylated across biological replicates with significant *P*-value (< 0.05) are annotated (Dataset EV1). Gene Ontology (GO) analysis suggested the major classes of proteins that exhibited altered phosphorylation were involved in the synthesis of lipids and metabolites such as sugars (Fig 1B). Interestingly, several trafficking-related proteins were also differentially phosphorylated in PfCDPK7-KO, including Rab11b, beta-coatamer, Sec61, and VPS18 (Fig 1A and C, and Dataset EV1).

Strikingly, the phosphorylation of ethanolamine kinase (EK) and phosphoethanolamine-N-methyltransferase (PMT) was altered significantly (Fig 1A and Dataset EV1, and Appendix Figs S1 and S3). EK phosphorylates ethanolamine to generate the phosphoethanolamine polar head group used for PE synthesis via the Kennedy pathway (Dechamps *et al*, 2010b). PfPMT is most closely related to plant orthologues (Dechamps *et al*, 2010a, 2010b) and is absent in *T. gondii* and in the rodent malaria parasite *P. berghei* (Ramakrishnan *et al*, 2013); this enzyme methylates phosphoethanolamine to generate phosphocholine, which can be used as a precursor for PC synthesis via the Kennedy pathway (Reynolds *et al*, 2008; Witola *et al*, 2008). These enzymes are thus implicated in PC and PE biosynthesis (Fig 2C) (Ramakrishnan *et al*, 2013), and the aforementioned observations were first indicators of a potential role of PfCDPK7 in the metabolism of these two PL classes. In addition, a phosphatidate phosphatase (PAP) homologue exhibited reduced phosphorylation in PfCDPK7-KO. PAP is putatively capable of generating diacylglycerol (DAG) from phosphatidic acid (PA), which is then used as the central precursor of PC and PE in the Kennedy pathway.

Protein–protein interaction (PPI) networks among the differentially phosphorylated proteins were predicted using the STRING database (Szklarczyk *et al*, 2015). The analysis indicated that the potential substrates or downstream effectors of PfCDPK7 might be involved in direct or indirect interactions with each other (Fig 1C and Appendix Fig S1). Some of these proteins were further shown to interact with PfCDPK7 using co-immunoprecipitation, which is discussed in the later sections.

PfCDPK7 disruption impairs phosphatidylcholine synthesis in *P. falciparum* asexual parasites

Since phosphorylation of proteins/enzymes involved in PL biosynthesis was significantly altered in PfCDPK7-KO line (Fig 1), we investigated if PfCDPK7 regulates phospholipid composition in *P. falciparum*. To this end, mass spectrometry-based lipidomics analyses were conducted on lipids extracted from wild-type 3D7 or PfCDPK7-KO. The analysis of the parasite phospholipid composition revealed a significant drop in total phosphatidylcholine (PC) content, whereas no other phospholipid class was significantly altered in the PfCDPK7-KO parasites (Fig 2A). As mentioned above, multiple pathways are involved in the synthesis of PC in *P. falciparum* (Fig 2C). Ethanolamine as well as choline can be utilized for the formation of PC. PfPMT enzyme is capable of generating phosphocholine from phosphoethanolamine, which is then used to generate PC via the regular Kennedy pathway (Reynolds *et al*, 2008; Witola *et al*, 2008).

To further validate the lipidomics data, the *de novo* synthesis of PC and PE via the parasite Kennedy pathway (Fig 2C) was

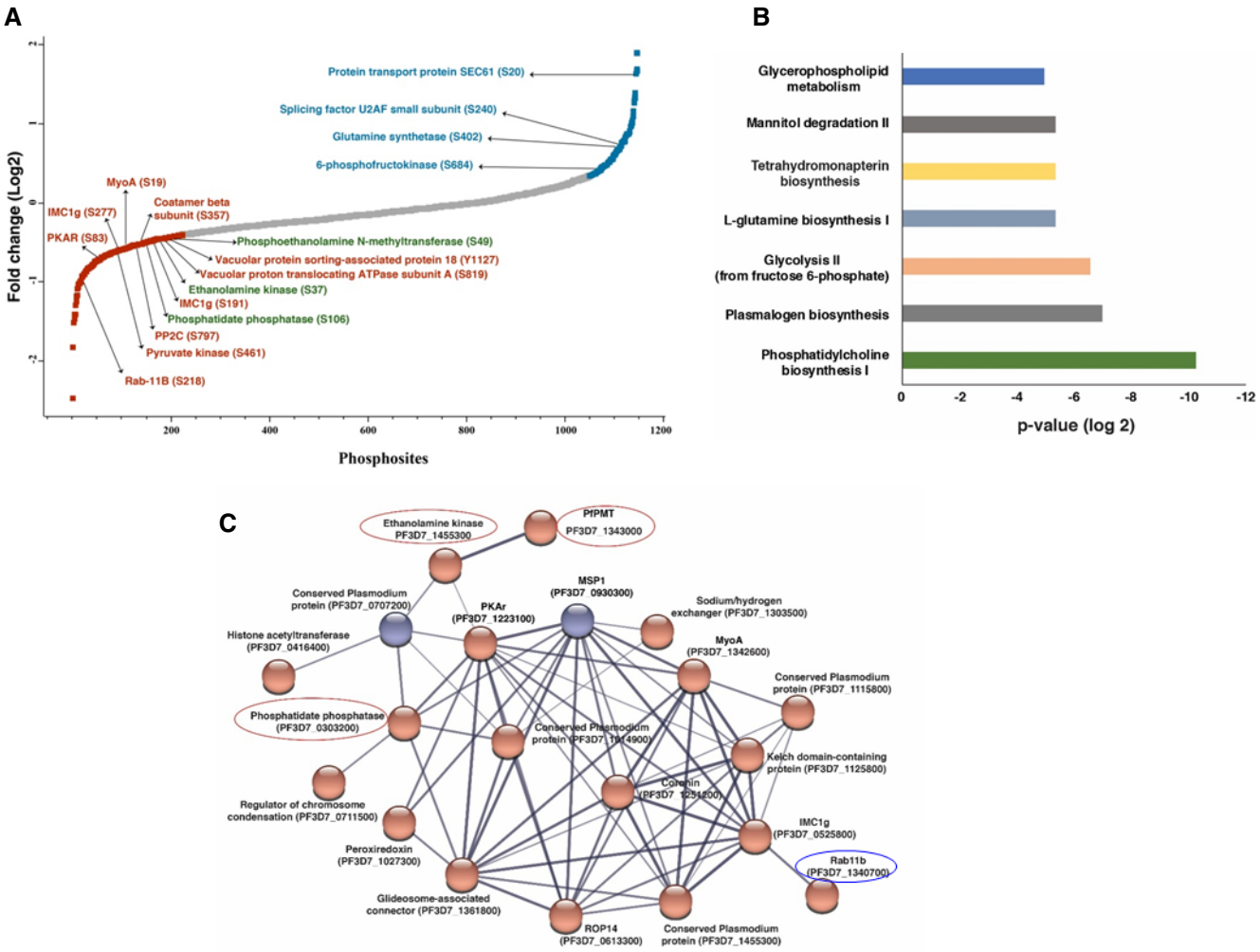

Figure 1. Comparative phosphoproteomics to identify processes regulated by PfCDPK7.

A Comparative phosphoproteomic and proteomic analyses were performed on late ring/early trophozoite stage wild-type (3D7) or PfCDPK7-KO parasites. The phosphorylation fold-change ratio of identified phosphopeptides was normalized to total protein abundance fold-change. The fold-change ratios for all phosphopeptides from various replicates are provided in Dataset EV1. The S-curve for the normalized data is provided for some of the significantly altered hyper- (blue) and hypo-(red) phosphorylated sites belonging to key proteins (Dataset EV1) are indicated. Phosphorylation sites of key enzymes involved in PL biosynthesis that exhibited reduced phosphorylation in PfCDPK7-KO parasites are indicated in green.

B Pathway analysis of proteins that exhibited reduced phosphorylation upon PfCDPK7 disruption and the possible metabolic pathways these proteins may regulate (Dataset EV1). The pathways are represented based on their *P*-values (log 2), as estimated by the gene ontology tool available at PlasmoDB.

C Protein–protein interactions were predicted between differentially phosphorylated proteins using the STRING resource. The analysis exhibited high confidence interactions between the candidate proteins (Appendix Fig S1 and Dataset EV1). A major signaling module that involved enzymes including EK and PMT implicated in PC/PE metabolism was identified, in addition to a network involving trafficking protein PfRab11b. Hyper- and hypophosphorylated proteins are indicated in blue and red respectively. Proteins that are relevant to the topic of this paper are encircled. Proteins involved in PL metabolism and trafficking are indicated in red and blue, respectively.

monitored by metabolic labeling and thin-layer chromatography (TLC). For this purpose, ^{14}C-Ethanolamine (Eth) and ^{14}C-Choline (Cho) were used as precursors of both PE and PC in intracellular parasites, respectively. Total lipids were extracted and labeled lipids were detected and quantified by high precision–thin-layer chromatography (HPTLC) (Fig 2D). Consistent with our data and previous analyses (Witola *et al*, 2008), ^{14}C-Eth labeling indicated the *de novo* synthesis of both PE and PC by using Eth (Fig 2D). While the change in PE levels was marginal and not significant, PC synthesis was significantly impaired in PfCDPK7-KO parasites (Fig 2D). Interestingly, the PC content was also reduced in PfCDPK7-KO when ^{14}C-Cho was used as the precursor (Fig 2D). These results are in agreement with our lipidomics analyses. Collectively, these data suggested that PfCDPK7 regulates PC biosynthesis in *P. falciparum*.

We also examined the fatty acid (FA) profile of PfCDPK7-KO parasites and compared it to that from the parental 3D7 line. Long polyunsaturated fatty acid (PUFA) chains were significantly reduced in PfCDPK7-KO parasites, and more specifically levels of

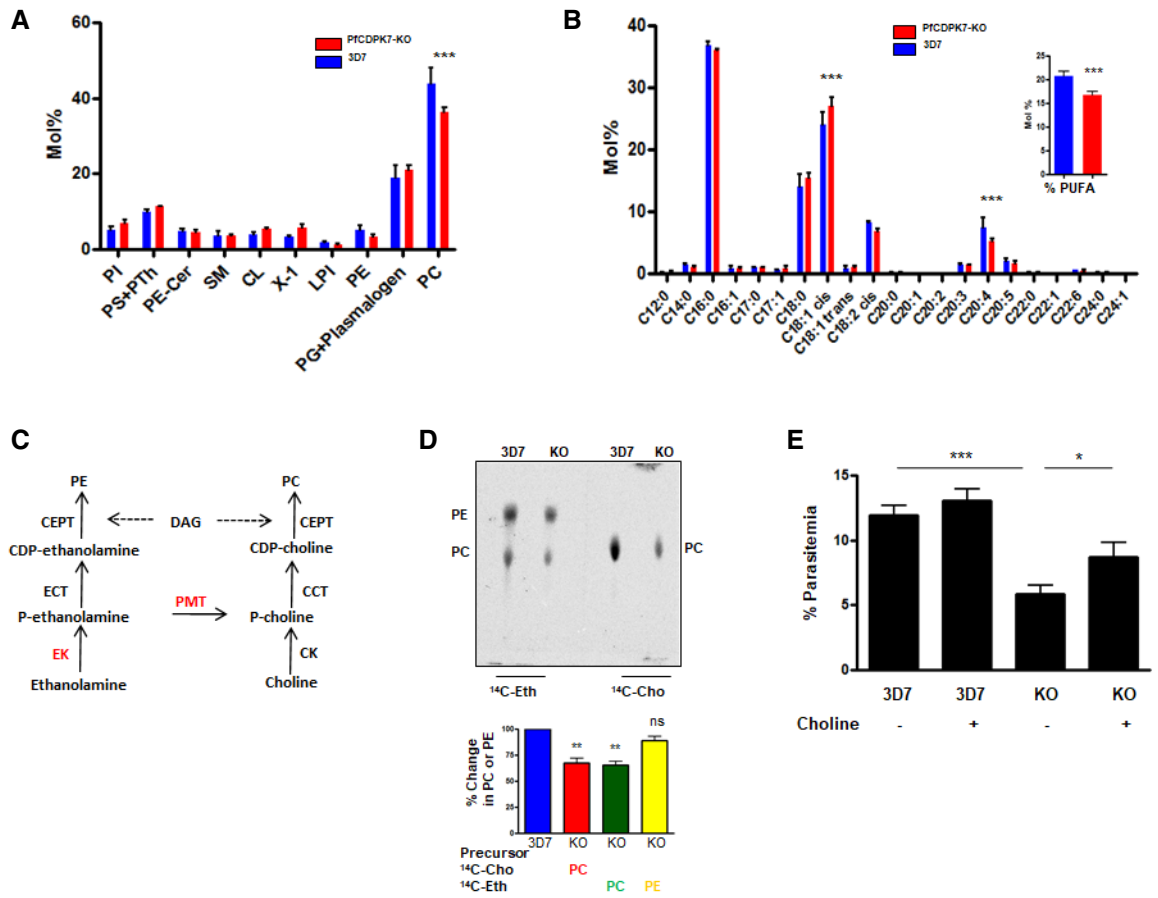

Figure 2. PfCDPK7 is involved in PC biosynthesis in *Plasmodium falciparum*.

A Total lipids were extracted from PfCDPK7-KO or 3D7 parasites and separated by HPTLC. After quantification by GC-MS content relative to total fatty acids was determined. Relative abundance of individual phospholipids was quantified. Disruption of PfCDPK7 caused a significant decrease in PC (mean ± SEM, $n = 3$; biological replicates, $^{***}P < 0.001$, *t*-test).

B Total fatty acids were extracted and separated before quantification by GC-MS analysis. The analysis shows an increase of C18:1 as well as the general decrease of PUFAs (inset) and more particularly C20:4 (mean ± SEM, $n = 3$; biological replicates, $^{***}P < 0.001$, *t*-test).

C Metabolic pathways depicting the synthesis of PC and PE in *P. falciparum*. PMT and EK, which are putative targets of PfCDPK7, are indicated in red (Ramakrishnan *et al*, 2013).

D Metabolic labeling to monitor PC and PE synthesis. Equal number of WT (3D7) and PfCDPK7-KO (KO) parasites were incubated with ^{14}C-Eth or ^{14}C-Cho (in RPMI) for 12 h. Subsequently, parasites were harvested and lipids were extracted and separated by thin-layer chromatography (TLC). The radiolabeled lipids were detected by phosphorimaging (upper panel). Bottom panel, radiolabeled PC and PE were quantitated by performing densitometry on phosphorimage of TLC plates in above panel and % change in PC or PE formation in PfCDPK7-KO parasites with respect to 3D7 (100%) was calculated (mean ± SEM, $n = 4$; biological replicates, $^{**}P < 0.01$, ANOVA; ns, nonsignificant).

E 3D7 or PfCDPK7-KO parasites were cultured in the presence or absence of 200 μM choline in culture medium. After 3 days, parasitemia was determined by counting parasites on thin blood smears (mean ± SEM, $n = 6$; biological replicates, $^{*}P < 0.05$, $^{***}P < 0.001$, ANOVA).

arachidonic acid, C20:4 (Fig 2B), while there was a slight significant increase in C18:1 cis species, likely reflecting overall changes in FA homeostasis and compensatory mechanisms. Long-chain PUFAs are mainly acquired from the host by blood-stage *P. falciparum* (Botte *et al*, 2013; Gulati *et al*, 2015), and our data suggested that FA uptake might thus be slightly impaired in PfCDPK7-KO parasites.

We determined the FA content of PC and PE; analysis of FA from PC suggested a decrease in C16:0 and a slight increase in C18:1 upon PfCDPK7 disruption (Appendix Fig S2A). However, PE from PfCDPK7-KO contained slightly higher C16:0 FA (Appendix Fig S2B). In contrast, C18:1 and C18:2 FA were significantly reduced. The PE levels do not change significantly in PfCDPK7-KO; therefore, the changes in FA do not seem to alter PE levels. It is possible that the altered phosphorylation of enzymes like EK and PMT (Fig 1A and C and Appendix Fig S3) that are directly involved in PC biosynthesis (Fig 2C) may contribute to the impairment of lipid metabolism in PfCDPK7-KO parasites. Supplementation of *P. falciparum* culture medium with exogenous choline can overcome growth defects caused by perturbation in PC biosynthesis (Reynolds *et al*, 2008; Brancucci *et al*, 2017). We complemented both parental and PfCDPK7-KO parasite lines with excess choline in culture medium and monitored the parasite growth. A moderate but significant

restoration of PfCDPK7-KO growth was observed suggesting that the loss of PC may impair parasite development in the absence of PfCDPK7 (Fig 2E). Taken together, our results suggest that PfCDPK7 is involved in regulating PC biosynthesis, which contributes to parasite development.

PfCDPK7 regulates PfPMT and PfEK

We next addressed the mechanisms through which PfCDPK7 regulates PC biosynthesis. Phosphoproteomic analysis revealed that PfCDPK7 knockout leads to reduced phosphorylation of PMT and EK (Fig 1A and Appendix Fig S3). First, we tested if PfCDPK7 interacts with these enzymes, by performing co-immunoprecipitation assays using parasite lysates, using a specific antisera raised against recombinant 6xHis-PMT. For studies related to EK, a parasite line overexpressing EK as a GFP fusion protein was generated and anti-GFP antibody was used to detect the EK-GFP fusion protein.

PfCDPK7 co-immunoprecipitated with both PMT (Fig 3A) and EK (Fig 3B), suggesting that PfCDPK7 may interact with EK and PMT in the parasite. This corroborated well with the data showing that they are hypophosphorylated at specific sites in PfCDPK7-KO parasites (Appendix Fig S3A and B).

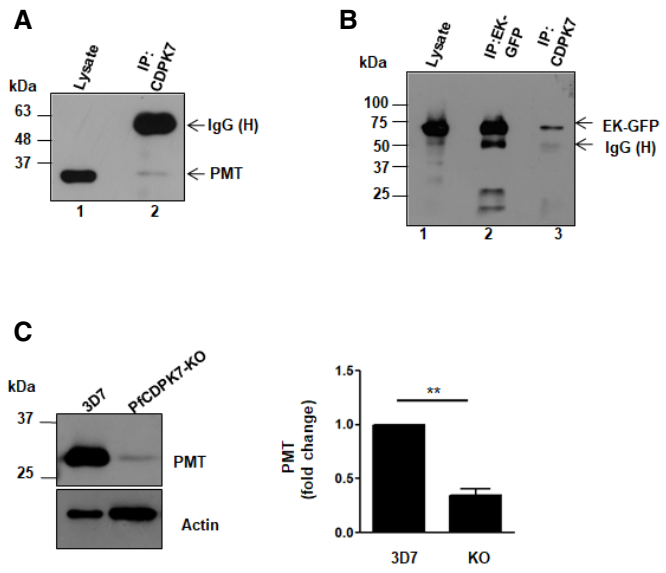

Figure 3. PfCDPK7 interacts with PMT and EK in the parasite and regulates PMT protein expression.

A, B 3D7 (A) or parasites overexpressing EK-GFP (B) were used to prepare protein lysates followed by immunoprecipitation using anti-PfCDPK7 or anti-GFP antibody, respectively. Subsequently, protein lysate or indicated IP were subjected to Western blotting using anti-PMT (A), anti-GFP (B). PMT was found to co-IP with PfCDPK7 (A, lane 2) and EK-GFP with PfCDPK7 (B, lane 3).

C 3D7 and PfCDPK7-KO parasites at schizont stage (~40 h) were used for Western blotting using anti-PMT antisera. Actin served as a loading control. Right panel: Densitometry was performed for bands corresponding to PMT in Western blots and the measurements were normalized to Actin. Fold change in PMT was determined with respect to 3D7 (mean ± SEM, $n = 4$; biological replicates, $^{**}P < 0.01$, t-test).

Source data are available online for this figure.

Interestingly, immunoblotting revealed that PMT protein levels (Fig 3C) were significantly lower in PfCDPK7-KO parasites. However, the levels of PMT transcript were almost unchanged (Appendix Fig S5), suggesting that PfCDPK7 may regulate PMT post-translationally, possibly by preventing its degradation. The aforementioned decrease in PMT phosphorylation in PfCDPK7-KO (Fig 1A) was particularly apparent on residue S49 (Appendix Fig S3A). IFA studies revealed that PfCDPK7 resides mainly in punctate structures (Appendix Fig S4A and B) as described previously (Kumar *et al*, 2014). Since PMT staining is spread throughout the parasite cytoplasm, it is difficult to determine if a pool of that protein co-localizes with PfCDPK7, although overlap can be observed (Appendix Fig S4B). EK-GFP was seen in the cytoplasm as well as in some punctate structures, which were often co-incidental with PfCDPK7 puncta (Appendix Fig S4A). Collectively, these data suggested that PfCDPK7 interacts with PMT and may participate in its regulation.

Phosphoproteomics indicated that the phosphorylation of EK S37 is decreased in PfCDPK7-KO parasites (Appendix Fig S3B). To further analyze the role of S37 phosphorylation, we generated parasite lines overexpressing a phospho-deficient (S37A) mutant of EK. The comparison of growth rates of parasites episomally overexpressing WT or EK-S37A mutant revealed that there was a significant decrease in the growth of parasites expressing the phosphomutant (Fig 4A). While analyzing the Giemsa smears, we noted that several S37A mutant-expressing parasites exhibited abnormal morphology and most of these abnormal parasites were at the ring to trophozoite transition or early trophozoite stage (Fig 4B). To investigate this further, IFAs were performed using antibodies against MSP1 and RAP1 as these proteins reside on the parasitophorous vacuole membrane (PVM) and in parasitophorous vacuole (PV) post-invasion, respectively (Riglar *et al*, 2011). Typically, WT EK-GFP parasites attained "round" or "amoeboid" shape 3–12 h post-invasion with MSP1 and RAP1 in close proximity as described previously (Kumar *et al*, 2014). In contrast, a significant number of S37A mutant expressing parasites possessed "abnormal" shapes in which fragmented or discontinuous MSP1 staining was observed (Fig 4C and D). In addition, blobs and extensions containing RAP1 were found in the host RBC outside the PV in infected erythrocytes (Fig 4C). These observations corroborated well with stunted mutant parasites observed on Giemsa-stained smears (Fig 4B). In addition to these defects, there was a significant reduction in the number of merozoites per schizont, which suggested defects in parasite replication (Fig 4E).

It is interesting to note that similar abnormalities were previously reported in the case of PfCDPK7-KO parasites, wherein the ring-trophozoite transition was hampered and similar stunted and abnormal parasites were observed and in addition parasite division was also impaired (Kumar *et al*, 2014). IFA studies revealed that wild-type EK-GFP was mainly cytoplasmic as reported previously for EK (Alberge *et al*, 2009). In addition, it also seemed to be present in punctate structures especially in mature parasites (Appendix Figs S4A and S6A). However, the EK S37A mutant protein was found mainly in the cytoplasm. Abnormal mutant parasites which exhibited defects in maturation of rings to trophozoites were also observed in these experiments, as indicated by the presence of minute amounts of hemozoin pigment (Appendix Fig S6A, lower panel), which is consistent with the observations performed on

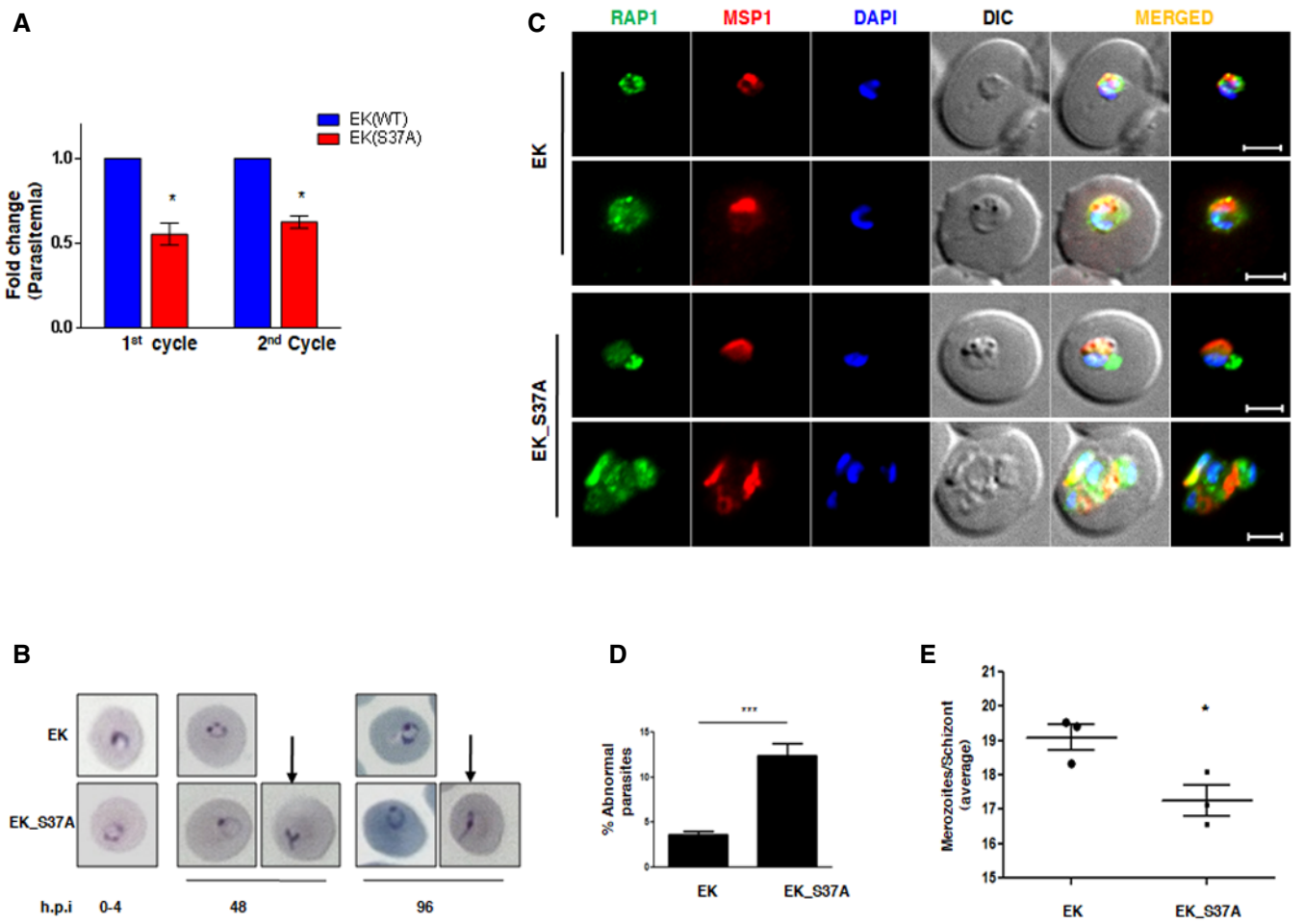

Figure 4. Phosphorylation of EK S37 is important for parasite development.

A Parasites overexpressing EK-GFP or its S37A mutant were synchronized and parasitemia was determined at the end of first (48 h.p.i) and second cycle (96 h.p.i). Fold change in parasitemia of EK_S37A parasites with respect to WT EK overexpressing parasites was compared, which was significantly reduced (mean ± SEM, $n = 3$; biological replicates, $^*P < 0.05$, ANOVA).

B Giemsa stained thin blood smears prepared at indicated hours post-infection (h.p.i) from assay. Arrows indicate parasites exhibiting abnormal morphology, which were observed at the beginning of each replication cycle.

C IFA was performed on parasites expressing WT EK-GFP or its S37A mutant 6–12 h post-invasion to detect (i) RAP1, which is transferred to PV post-invasion, and (ii) MSP1 which is located at the PVM. Parasite expressing WT EK-GFP exhibited typical round ring like shape. In contrast, several parasites expressing the S37A mutant exhibited irregular morphology with much smaller vacuolar space and in some parasites RAP1 was found outside the PV (Scale bar, 1 μm).

D Quantitation of abnormal parasites in IFA described in panel C (mean ± SEM, $n = 3$; biological replicates, $^{***}P < 0.001$, t-test).

E Parasites EK-GFP or its S37A mutant were synchronized and parasites were allowed to mature to schizonts/segmentors. The graph shows average number of merozoites per schizont from three biological replicates. Each replicate represents an average of merozoites from 30–40 schizonts. (mean ± SEM, $n = 3$; biological replicates, $^*P < 0.05$, t-test).

Giemsa smears (see above) (Fig 4B). Moreover, Western blotting suggested that EK protein levels remain same in EK-WT and EK-S37A mutant parasites (Appendix Fig S6B).

Taken together, these results established that PfCDPK7-mediated regulation of the key PC biosynthetic pathway enzymes PMT and EK plays an important role in parasite development.

PfPI4K regulates the localization of PfCDPK7

Our previous observations suggested that PfCDPK7 interacts with 4'-phosphorylated phosphoinositides, in particular PI(4,5)P_2 using a dot blot assay (Kumar *et al*, 2014). These PIPs interact with the PH domain of the kinase and guide its cellular localization, which is likely to be critical for its function (Kumar *et al*, 2014). Given that PI4-kinases are involved in the generation of 4'-PIPs in eukaryotic cells (Balla, 2013) including *Plasmodium* (McNamara *et al*, 2013; Paquet *et al*, 2017), we set out to investigate the role of PfPI4K in PfCDPK7-dependent processes.

Typically, PIPs regulate their effectors by guiding their localization to desired cellular compartments or their site-of-action (Lemmon & Ferguson, 2001; Lemmon, 2003), which was the case with PfCDPK7 (see above) (Kumar *et al*, 2014). Pharmacological PfPI4K

inhibitors have been developed in the last few years (McNamara *et al*, 2013; Paquet *et al*, 2017; Brunschwig *et al*, 2018), and one of them, MMV39048 (referred subsequently as MMV048), displayed potent anti-malarial activity against almost all stages of parasite development, subsequently progressed to clinical trials (McCarthy *et al*, 2020). Another, more potent analogue of this series, UCT943, was recently developed (Brunschwig *et al*, 2018). In addition to being candidate drugs, these compounds also represent useful research tools to investigate the effects of a block in 4'-PIP formation in live parasites (Paquet *et al*, 2017; Brunschwig *et al*, 2018). However, despite PfPI4K being a validated target for antimalarials that have reached clinical trials, the molecular mechanisms by which PfPI4K and its inhibitors may regulate parasite development have remained unclear.

IFA studies were performed to assess the effect on PfCDPK7 cellular localization. Treatment with both UCT943 and MMV048 resulted in a dramatic change in PfCDPK7 localization, from punctate vesicular structures present in the vicinity of the ER as described previously (Kumar *et al*, 2014) to a diffuse cytoplasmic distribution accompanied by a loss of PfCDPK7-associated vesicles (Fig 5A). However, PfPI4K inhibition did not alter PfCDPK7 expression (Fig 5B). These data indicated that PfPI4K product 4'-PIPs regulate PfCDPK7 subcellular localization; since correct cellular localization is likely to be critical for its function, the absence of 4'-PIPs may lead to dysregulation of PfCDPK7 activity, contributing to the mode of action of the PfPI4K inhibitors.

PfPI4K inhibitors prevent PL biosynthesis in the parasite and cause degradation of PfPMT and PfEK

PfPI4K inhibitors have previously been shown to dramatically suppress parasite growth (Paquet *et al*, 2017; Brunschwig *et al*, 2018). Given that both PfCDPK7-KO (Kumar *et al*, 2014) and EK S37A phosphomutant parasites exhibit defects in the ring to trophozoite transition (Fig 4B and C), it was pertinent to determine if PfPI4K, which acts upstream of PfCDPK7, influences this process. MMV048 treatment caused defects in PVM/PM development, as indicated by aberrant RAP1 localization (Fig 5C), which was also observed in both PfCDPK7-KO (Kumar *et al*, 2014) and EKS37A-mutant parasites (Fig 4C).

To determine the effect of PfPI4K inhibition on PL biosynthesis, we treated parasites with 5–25 nM UCT943 and 25–50 nM MMV048, which is in the range of IC50 against NF54 strain (Paquet *et al*, 2017; Brunschwig *et al*, 2018). Subsequently, metabolic labeling of PLs was performed using ^{14}C-choline or ^{14}C-ethanolamine as described above for PfCDPK7-KO parasites. TLC analysis revealed that there was a dose dependent decrease in PC synthesis from both choline and ethanolamine (Appendix Fig S7). Furthermore, PE biosynthesis was also affected in UCT943-treated (Appendix Fig S7B) and MMV048-treated parasites (Appendix Fig S7A). Subsequent experiments were performed with 10 and 50 nM of UCT943 and MMV048, respectively, as optimal inhibition in PC/PE formation was observed at this concentration (Fig 6A and B). These data suggested that PfPI4K regulates PC biosynthesis, presumably through its ability to regulate PfCDPK7. In addition, it also regulates PE biosynthesis (Fig 6B).

As mentioned above, EK and PMT were hypophosphorylated in PfCDPK7-KO parasites and phosphorylation seems to regulate the levels of PMT (Figs 1A and 3C). Therefore, it was of interest to test if UCT943 and MMV048 treatment affected these enzymes. Strikingly, inhibitor treatment depleted PMT protein as revealed by Western blotting (Fig 6C), corroborating with the impaired PMT expression in PfCDPK7-KO parasites (Fig 3C) and supporting the hypothesis that PfPI4K may regulate PMT via PfCDPK7. To assess the effect of PfPI4K inhibition on EK, parasite line overexpressing EK-GFP was treated with the inhibitors. Both inhibitors caused a significant degradation of both PfEK and PfPMT (Fig 6C and D). These data correlate well with the loss of PC and PE in parasites treated with PfPI4K inhibitors and are consistent with a role of PfPI4K/PI4P signaling in PL biosynthesis.

PfPI4K and PfCDPK7 may regulate TVN formation

Tubulovesicular networks (TVNs) are extensions of the PVM into the host RBCs used by the parasite for the acquisition of nutrients from the extracellular milieu (Elmendorf & Haldar, 1994; Lauer *et al*, 1997). Although parasite sphingomyelin synthase (SMS), which uses ceramide for sphingomyelin (SM) synthesis, was shown to contribute to the formation of the TVNs, it is likely that other PLs contribute to this process. Given that PfPI4K and PfCDPK7 regulate PC/PE biosynthesis, it was of interest to test their role in TVN biogenesis.

BODIPY-Ceramide can be used to label contiguous TVNs, which extended into the host RBC cytoplasm in the case of wild-type parasites (Elmendorf & Haldar, 1994). Treatment of ring-stage parasites with PfPI4K inhibitors followed by BODIPY-Ceramide labeling (Fig 7A) revealed a marked disruption in the formation of TVNs, with parasites exhibiting smaller vesicles or no extensions from the PVM (Fig 7A). To test if the uptake of extracellular molecules may be altered, we used FM4-64, a fluorescent lipophile probe that naturally stains plasma membrane and which can be imported from the RBC plasma membrane by *P. falciparum* TVN (Lauer *et al*, 1997, 2000). Indeed, the endocytosis of FM4-64, which relies on TVNs, was also impaired significantly in MMV048-treated parasites (Fig 7B).

The formation of TVNs was also investigated in PfCDPK7-KO parasites. In contrast to wild-type parasites, the TVNs were stunted as indicated by either shortened size and/or fragmented vesicular structures in PfCDPK7-KO (Fig 7C). PfCDPK7-KO parasites also exhibited a drastic reduction in FM4-64 internalization (Fig 7D), which was most likely due to stunted TVNs. These data corroborate well with the fact that PfPI4K inhibitors also cause similar defects and suggest that PfPI4K signaling via PfCDPK7 may regulate TVN formation. We did not observe a significant change in sphingomyelin levels in PfCDPK7-KO parasites (Fig 2A). It is possible that PC, which is a major PL in *Plasmodium,* may also contribute to TVN formation (Figs 2 and 6), which is possibly one of the reasons for impaired TVN formation in PfCDPK7-KO and PfPI4K inhibitor-treated parasites.

Discussion

We have identified a PfCDPK7-dependent signaling pathway in *P. falciparum* (Fig 8). One of the features revealed by comparative phosphoproteomics was the altered phosphorylation of key

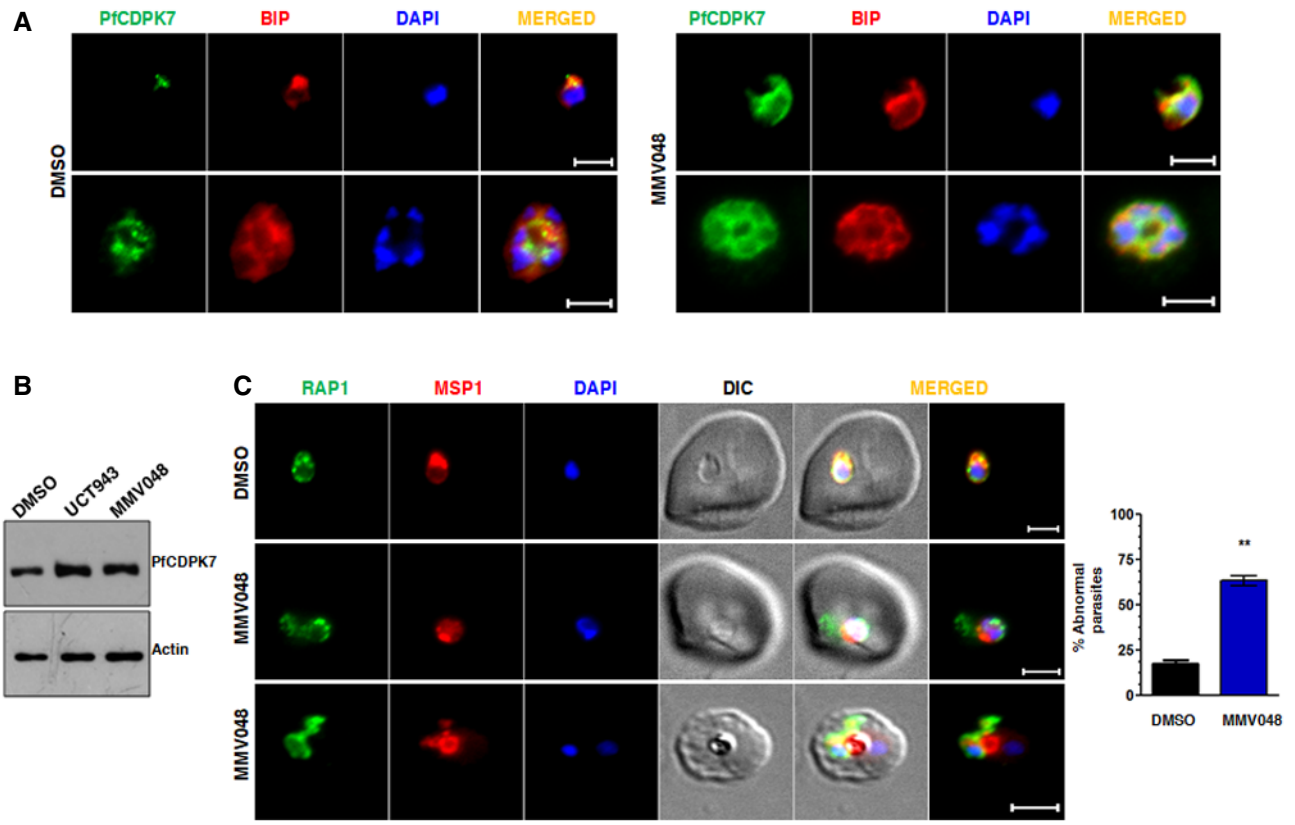

Figure 5. PfPI4K is involved in the localization of PfCDPK7 and parasite maturation.

A 3D7 parasites were treated with DMSO or 50 nM MMV048 for 24 h. Subsequently, parasites were fixed and IFA was performed to detect ER marker BiP and PfCDPK7. While PfCDPK7 was present in puncta proximal to ER (left panel), inhibitor treatment caused a loss in this vesicular localization and resulted in a more diffuse distribution of the enzyme (right panel) (Scale bar, 1 μm).

B Western blotting was performed on parasites treated with DMSO, 10 nM UCT943 or 50 nM MMV048 as described above using anti-PfCDPK7 or anti-Actin (loading control) antibody. Please note that this protein lysate was also used for Western blots in Fig 6C with other antibodies. Therefore, this loading control blot for actin shown here pertains to the loading control in Fig 6C as well.

C 3D7 parasites were treated with DMSO or 50 nM MMV048 for 20–24 h. Subsequently, IFA was performed ~24 h post-invasion to detect RAP1 and MSP1 (left panel) as described in Fig 4C. Right panel, quantitation of parasites exhibiting abnormal staining for RAP1 outside the PV was observed (mean ± SEM, $n = 3$; biological replicates, $^{**}P < 0.01$, *t*-test; Scale bar, 1 μm).

Source data are available online for this figure.

enzymes in the biosynthesis of PLs in PfCDPK7-KO parasites. In line with this observation, PC biosynthesis was significantly impaired in these parasites (Fig 2A and D). Interestingly, we found that PfPMT expression was markedly reduced in PfCDPK7-KO parasites (Figs 3C and 8), which corroborated well with the observed reduced PC biosynthesis from Eth (Fig 2A and D). Interestingly, the knockout of PfPMT also caused defects in parasite maturation and replication (Witola *et al*, 2008), as was the case with PfCDPK7-KO (Kumar *et al*, 2014). Recently, LysoPC depletion from serum was shown to cause defects in metabolism of PC via the Kennedy pathway and induced commitment to sexual differentiation (Brancucci *et al*, 2017). Interestingly, expression of transcripts for PfCDPK7, along with mRNAs encoding EK, PMT, and other enzymes implicated in PC synthesis, was enhanced upon LysoPC depletion (Brancucci *et al*, 2017), which was possibly a response by the parasite to activate its machinery for PC synthesis. Conversely, Lyso PC depletion abrogated asexual division, which is consistent with present findings. It will be of great interest to examine phenotypes of PfCDPK7-KO parasites in sexual development.

Phosphoproteomic analysis revealed impaired phosphorylation of EK at S37 in PfCDPK7-KO parasites; moreover, PfCDPK7 and EK co-immunoprecipitated, suggesting that they may interact in the parasite facilitating EK phosphorylation. The overexpression of S37A mutant of EK caused abnormal parasite morphology, possibly because of altered PVM/PM formation (Fig 4C and Appendix Fig S6A). In addition, parasite division was also impaired upon mutant overexpression (Fig 4E). Interestingly, similar defects were previously observed in PfCDPK7-KO parasites (Kumar *et al*, 2014) strengthening the notion that PfCDPK7 and EK function in the same pathway (Fig 8).

Given that EK is involved in the synthesis of both PC and PE (Fig 2C), it was surprising that PfCDPK7-KO exhibited decrease mainly in PC. Based on the predicted capacity of *P. falciparum* to generate lipids *de novo*, it is possible that reduced levels of

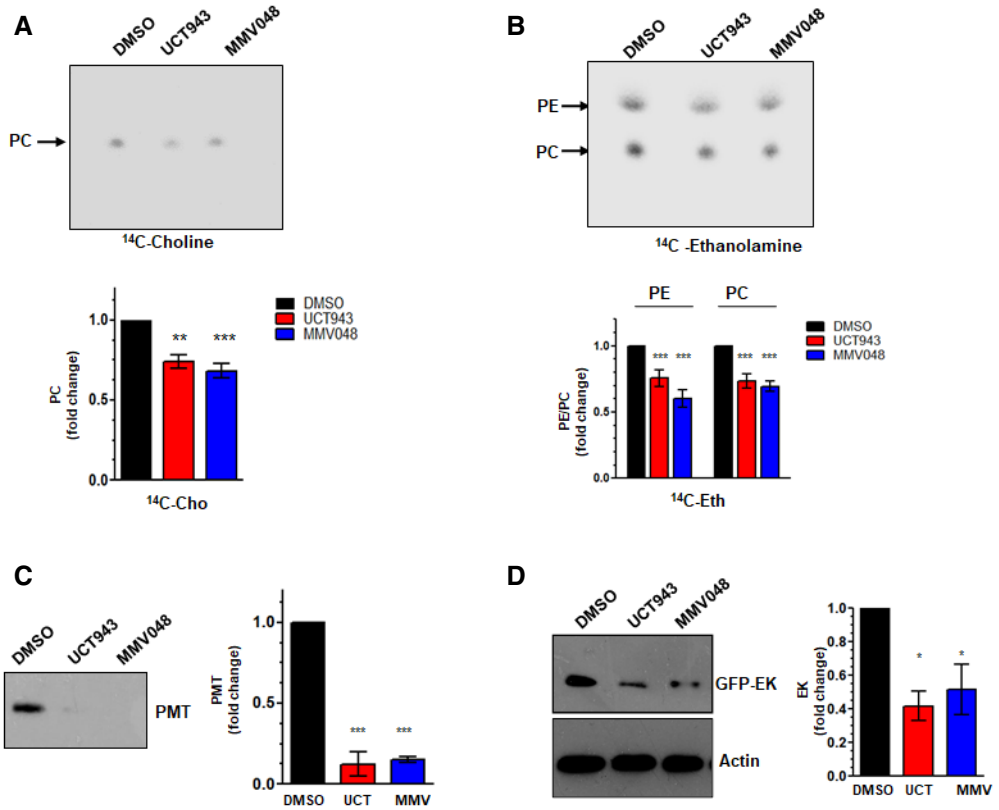

Figure 6. PfPI4K inhibitors impair PL biosynthesis.

A, B 3D7 parasites were synchronized and treated with 10 nM UCT943 or 50 nM MMV048 for 10–12 h. Subsequently, parasites were incubated with ^{14}C-Cho (A) or ^{14}C-Eth (B) and were harvested after 12 h. Total lipids were extracted and separated by TLC. The radiolabeled lipids were detected by phosphorimaging and quantitated by densitometry (upper panel). Bottom panel (A and B), fold change in PC and PE formation in inhibitor-treated parasites with respect to DMSO treatment was determined (mean ± SEM, $n = 4$; biological replicates, $^{**}P < 0.01$, $^{***}P < 0.001$, ANOVA; ns, not significant).

C, D UCT943 and MMV048 treated 3D7 (C) or EK-GFP overexpressing parasites (D) were subjected to Western blotting (as described in Fig 5B) using anti-PMT (C) and anti-GFP (D) antibodies (left panels). For experiments in Fig 6C, the lysate used was the same as the one used for Fig 5B for PfCDPK7 Western blotting. Therefore, the corresponding actin blot for loading control is shown in Fig 5B. Right Panels: densitometry was performed for bands corresponding to PMT (C) or EK-GFP (D), which were normalized with respect to Actin. Fold change in PMT or EK was determined with respect to DMSO treated parasites (Mean ± SEM, $n = 4$; biological replicates, $^{*}P < 0.05$, $^{***}P < 0.001$, ANOVA).

Source data are available online for this figure.

phosphoethanolamine are caused due to impaired EK phosphorylation. As a result, phosphoethanolamine may be limiting for the utilization by the PMT (Fig 2C and D). Given that PMT is involved in the trimethylation of phosphoethanolamine to form phosphocholine, which is an intermediate in PC biosynthesis (Fig 2C), its regulation by PfCDPK7 would further affect PC biosynthesis (Figs 2D and 8). Collectively, these data strongly suggest that PfCDPK7 regulates the synthesis of PC by regulating enzymes like PMT and EK that are involved in its biosynthesis (Fig 8). Previous results including ours show that synthesis of PC is an important metabolic nexus and that the parasite has acquired multiple metabolic route to achieve it in any circumstances including physiological variations in the host. The presence of a plant-like PMT in *P. falciparum* is one such example, which allows the parasite to obtain more PC via this metabolic pathway when required, although usually less essential (Witola *et al*, 2008). Our results confirm that there are important regulatory pathways to make sure that parasite generates enough PC and PfCDPK7 is part of that regulation loop. The fact that there was a decrease in PC formation using both Eth and Cho as precursor in PfCDPK7-KO parasites (Fig 2D) suggests that PfCDPK7 may influence formation of PC via both these pathways, which it may achieve by regulating PMT, EK, and other additional targets.

To our knowledge, these are first observations that directly link protein phosphorylation to PL biosynthesis in *Plasmodium*. Our results are also consistent with the observation that the disruption of CDPK7 in the related apicomplexan parasite *Toxoplasma gondii* solely induces a significant reduction of PE levels, but does not affect those of PC (Bansal *et al*, 2021). Of note, *T. gondii* does not possess a PMT to allow the conversion of phosphoethanolamine to phosphocholine, unlike *P. falciparum* (Bansal *et al*, 2021). Moreover, EK was not identified as a TgCDPK7 target in *T. gondii* and EK S37 is not conserved in the *Toxoplasma*. Instead, enzymes like glycerol-3-phosphate acyltransferase (TgGPAT) and phosphatidic acid phosphatase (PAP) were found to be regulated by TgCDPK7, which it may contribute to the regulation of PE biosynthesis in *T. gondii*. Interestingly, TgCDPK7 target sites on these enzymes in

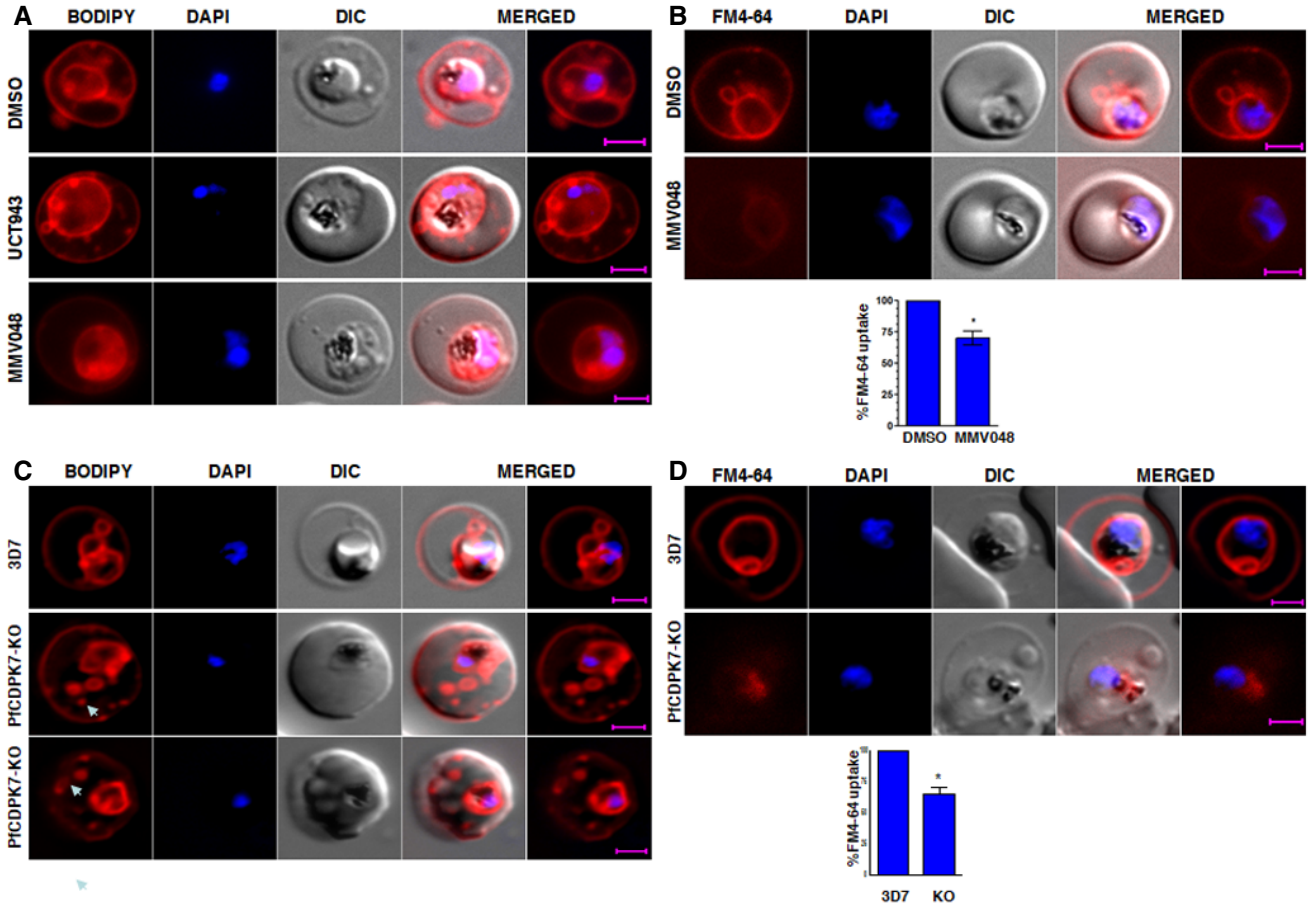

Figure 7. PfPI4K and PfCDPK7 may regulate TVN formation and endocytosis.

A 3D7 ring-stage parasites were treated with DMSO or UCT943 or MMV048 for 20–24 h, washed with HBSS before incubation with BODIPY-ceramide and DAPI followed by live imaging. TVN formation seemed to be impaired upon inhibitor treatment (Scale bar, 1 μm).

B Ring-infected erythrocytes were treated with MMV048 for 24 h and then incubated with FM4-64 and DAPI to assess lipid uptake. Subsequently, FM4-64 associated fluorescence was detected by fluorescence microscopy (upper panel) or quantitated by FACS (lower panel) and % change in FM4-64 uptake in inhibitor-treated parasites was determined. (mean ± SEM, $n = 3$; biological replicates, $^*P < 0.05$, t-test; Scale bar, 1 μm).

C Synchronized PfCDPK7-KO or 3D7 ring/trophozoite stage parasites were labeled with BODIPY-ceramide and DAPI followed by live imaging as described for panel A. While tubular vesicular networks/structures (TVNs), vesicles were predominantly labeled in 3D7 parasites, most PfCDPK7-KO parasites did not exhibit TVN; instead, small punctate spots (white arrowheads) were seen in the iRBC cytoplasm (Scale bar, 1 μm).

D Trophozoite stage infected erythrocytes were incubated with FM4-64 and DAPI to assess lipid uptake by 3D7 or PfCDPK7-KO parasites. Subsequently, FM4-64 associated fluorescence was visualized by live microscopy (top panel) and also analyzed by FACS and % change in FM4-64 uptake in KO parasites was determined (bottom panel) (mean ± SEM, $n = 3$; biological replicates, $^*P < 0.05$, t-test; Scale bar, 1 μm).

T. gondii are not conserved in the *Plasmodium* homologues. These differences in the biosynthesis of different PLs highlight the evolutionary and metabolic plasticity that exists in PL synthesis pathways. Comparative phosphoproteomics studies also revealed that PfCDPK7 may target proteins involved in trafficking (Fig 1A and C), which includes PfRab11b. Interestingly, TgRab11a (but not TgRab11b) was identified as a TgCDPK7 target in previous studies, and its phosphorylation was shown to be critical for its function in parasite division (Bansal *et al*, 2021). The regulation of PfRab11b isoforms and other putative trafficking protein targets by PfCDPK7 will be of great interest for future studies (Fig 8).

Experiments with the PI4K inhibitors UCT943 and MMV048 reveal that PfPI4K and 4'PIPs are implicated in PL biosynthesis. PfCDPK7 interacts with PIPs via its PH domain, which is critical for the localization of the kinase to vesicular compartments that are proximal to the ER (Kumar *et al*, 2014). The inhibition of PfPI4K impaired the localization of PfCDPK7 to these vesicular organelles (Fig 5A), confirming that its products 4'-PIPs regulate PfCDPK7 cellular localization (Fig 8). Several defects observed in PfCDPK7-KO and PfPI4K inhibitor-treated parasites were similar: parasite maturation, PL biosynthesis, PMT expression, and TVN formation. PfPI4K seems to regulate the formation of both PC and PE suggesting that in addition to PfCDPK7 (which contributes to PC formation), it may have other targets that may regulate PE formation. PfPI4K inhibition resulted in the degradation of PfEK and PfPMT (Fig 6C and D), which explained the loss of PC and PE (Fig 6A and B).

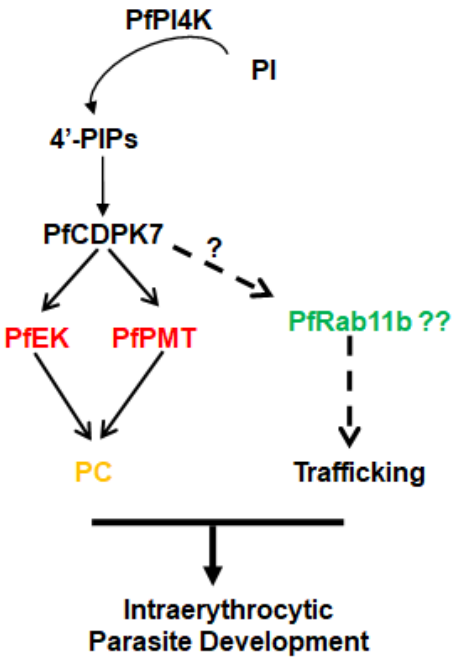

Figure 8. A simplified model of PfPI4K-PfCDPK7 signaling in *Plasmodium falciparum*.

4'-phosphorylated phosphoinositides (4'-PIPs) generated by PfPI4K interact with the PH domain of PfCDPK7 (Kumar *et al*, 2014) and regulate the localization and thereby the function of PfCDPK7 (Fig 5A), which in turn promotes the synthesis of phosphatidylcholine (PC) (Fig 2A and D) by regulating enzymes (indicated in red) like ethanolamine kinase (PfEK) and phosphoethanolamine methyltransferase (PfPMT) (Figs 3 and 4) that are involved in PL metabolism (Fig 2C). In addition, phosphoproteomics suggest that PfCDPK7 may contribute to vesicular trafficking via effectors (indicated in green) like PfRab11b but this pathway needs further investigation (Fig 1A and C). Collectively, these events regulate intraerythrocytic development of the parasite.

TVNs are critical for the uptake of nutrients by the parasite from the extracellular milieu. Sphingomyelin synthase (SMS) inhibitors prevent the formation of TVN (Lauer *et al*, 1997). While we did not observe any significant change in SM levels in PfCDPK7-KO parasites (Fig 2A), TVN formation was abrogated in both PfCDPK7-KO and PfPI4K inhibitor-treated parasites. It is reasonable to suggest that PLs such as PC/PE may also contribute to TVN formation, which is a possible reason for its impairment in these parasites. As a result, uptake of nutrients by the parasite may be impaired, resulting in stalled growth and division, which may contribute to the mode of action of the PfPI4K inhibitors. As mentioned above, long-chain PUFA were significantly reduced in PfCDPK7-KO parasites (Fig 2B). Long-chain PUFAs are mainly acquired from the host by blood-stage *P. falciparum* (Botte *et al*, 2013; Gulati *et al*, 2015) further suggesting that PfCDPK7 may regulate lipid trafficking scavenged from the host. Although the role of TVNs in FA uptake is not clear, it is possible that impaired TVN formation contributes to this process.

PfPI4K has been identified as a major antimalarial drug target (McNamara *et al*, 2013; Brunschwig *et al*, 2018; McCarthy *et al*, 2020), and MMV048 is being tested in human clinical trials as a novel anti-malarial (McCarthy *et al*, 2020). However, its mechanism of action has remained unknown. The data we present here provide insights into at least one of the pathways through which PI4K signaling regulates parasite development (Fig 8).

Materials and Methods

Materials

All chemicals and oligonucleotides were purchased from Sigma-Aldrich unless indicated otherwise. Roswell Park Memorial Institute medium (RPMI) 1640, and Albumax II were purchased from Gibco (Thermo Fisher Scientific, USA). Antibodies were procured from Santa Cruz Biotechnology (mouse anti-β-actin, sc-47778, 1:1,000 for Western blotting), and Roche (anti-GFP, 1:200 for IFA). PfCDPK7 antisera has been described previously (Kumar *et al*, 2014). Horseradish peroxidase-labeled secondary goat anti-rabbit/mouse antibodies and Alexa Fluor 488- and Alexa Fluor 594-conjugated goat anti-mouse/rabbit antibodies were obtained from Molecular Probes. MMV390048 (MMV048) was a kind gift from Medicines in Malaria Venture and UCT943 was gifted by Dr. Kelly Chibale, University of Cape Town.

Proteomics studies

Cell lysis and protein extraction

3D7 or PfCDPK7-KO parasites were cultured (see below) (Kumar *et al*, 2014) and were synchronized using sorbitol. As described in our previous study (Kumar *et al*, 2014), PfCDPK7-KO parasites exhibit first defects in development during ring-trophozite transition (~20 h post-invasion). However, such "abnormal" parasites are observed in second and subsequent life cycle. Since the parasites used in present studies were normalized after synchronization (~4 h post-invasion), they were largely of similar stages and healthy at ~20 h post-invasion for reported studies. Therefore, parasites at this late ring/early trophozoite stage were used for phosphoproteomic and lipidomics (see below) analysis. Parasites were harvested after saponin lysis of infected RBCs. The parasite pellet was washed and were dissolved in protein extraction buffer (50 mM triethylammonium bicarbonate (TEABC), 8 M urea, 1 mM sodium orthovanadate, 1 mM sodium fluoride, 1 mM β-glycerolphosphate, 2.5 mM sodium pyrophosphate) followed by sonication. The lysate was centrifuged and the supernatant containing the proteins was used for bicinchoninic acid assay-based protein estimation. Equal amount of protein was taken from PfCDPK7-KO and wild-type 3D7 samples and subjected to reduction (20 mM dithiothreitol, 60°C for 30 min) and alkylation (20 mM iodoacetamide, ambient temperature for 10 min in dark). Proteins were then digested using trypsin (Promega, Madison, USA) in 1:20 enzyme to protein ratio. Digested peptides were lyophilized and used for iTRAQ labeling.

iTRAQ labeling, peptide fractionation, and phosphopeptides enrichment

iTRAQ labeling was performed on ~3 mg of dried peptides from PfCDPK7-KO and wild-type parasites, as per the manufacturer's instructions. Labeling efficiency was estimated by analyzing 2 μg equivalent of labeled peptides on the mass spectrometer. Upon successful labeling, peptides from mutant and wild-type parasites were pooled and dried. Sample labeling information is provided in

Table EV1. Peptides were fractionated using basic reverse-phase liquid chromatography (bRPLC) and fractionation was carried out on Xbridge C18, 5 μm 250 × 4.6 mm column (Water Corporation, Milford, USA) as described earlier (Bansal *et al*, 2021). A gradient of 5–60% of solvent B (10 mM TEABC, pH 8.3 in 95% acetonitrile) for 60 min was used with a flow rate of 1 ml/min. A total of 96 fractions were collected that were concatenated into 12 fractions and dried. Approximately 10% aliquot from each fraction was used for the total proteome analysis and the remaining fraction was processed for TiO_2-based enrichment of phosphopeptides.

Peptide mixtures were reconstituted in 250 μl of 5% dihydroxybenzoic acid in 80% acetonitrile and 3% trifluoroacetic acid (TFA). Titansphere beads (GL Sciences, Japan) were mixed with dissolved peptides in 1:1 ratio and incubated for 1 h at room temperature. Unbound peptides were washed off with 80% acetonitrile in 3% TFA (twice) and bound peptides were eluted with 4% ammonium solution. Eluted peptides were then dried and desalted using C18 stage tips.

LC-MS/MS data analysis

LC-MS/MS analysis was carried out using Orbitrap Fusion mass spectrometer interfaced with Proxeon Easy-nLC 1000 system (Thermo Scientific, Bremen, Germany). Each fraction from total proteome and phosphopeptides enriched samples was reconstituted in 0.1% formic acid and loaded on 2 cm long pre-column packed with C18 material. Subsequently, eluted peptides were further resolved on analytical column (75 μm × 25 cm, C18, 3 μ particle size) and were eluted by passing 0.1% formic acid in 80% acetonitrile (Solvent B) for 120 min gradient with flow rate of 300 nl/min. The data were acquired in data-dependent acquisition (DDA) mode. The precursor ions were acquired in full MS scan mode in a range of 400–1,600 m/z, with Orbitrap mass analyzer resolution of 120,000 at 200 m/z. Automatic gain control (AGC) target value was set to 2 million with an injection time of 50 ms and dynamic exclusion of 30 s. The most intense precursor ions were selected at top speed data-dependent mode with 3 s cycle time and were isolated using quadrupole with isolation window of 2 m/z and isolation offset of 0.5 m/z. These filtered precursor ions were fragmented using higher energy collision-induced dissociation (HCD) with 34 ± 3% normalized collision energy. MS/MS scans were acquired in centroid mode for range of 110 to 2,000 m/z in Orbitrap mass analyzer with mass resolution of 30,000 mass resolution at 200 m/z. AGC target was set to 50,000 with an injection time of 54 ms. MS/MS data were acquired in technical duplicates.

Data analysis

MS/MS raw data were searched against a combined protein database of *P. falciparum* 3D7 (downloaded from PlasmoDB web resource) and humans using search engines Sequest and Mascot (version 2.4.1) through Proteome Discoverer version 2.2 software (Thermo Fisher Scientific). Trypsin was selected as the protease enzyme with a maximum of two missed cleavages. A precursor mass tolerance and fragment mass tolerance of 10 ppm and 0.05 Da were selected, respectively. Carbamidomethylation at cysteine and iTRAQ labeling at lysine and N-terminus of peptide were selected as static modifications. In dynamic modifications, oxidation of methionine and phosphorylation at serine, threonine, and tyrosine were included. Data were filtered at 1% FDR at PSM level. The phosphorylation fold changes were normalized against the total proteome data as mentioned earlier (Kumar *et al*, 2017). The ptmRS node was enabled during the search to calculate the probability of phosphorylation site localization and a ptmRS score ≥ 75% was used as a cutoff.

List of phosphopeptides along with their fold changes (mutant/control) from four biological replicates were uploaded on Perseus software (version 1.4) to calculate *P*-value (Student *t*-test) for each phosphosite and to generate the S-curve. We further applied the fold change cutoff of 1.33 to filter differentially phosphorylated sites based on our observations in previous study (Kumar *et al*, 2017). GO analysis was carried out through PlasmoDB web resource. For the prediction of protein–protein interactions, STRING web resource (version 10.0) was used. Proteins that were found to be differentially phosphorylated were considered for the analysis, and interactions were predicted with medium confidence filter (Szklarczyk *et al*, 2011).

Generation of parasite lines overexpressing EK-GFP or its S37A mutant

To generate EK-GFP overexpression construct, *EK* cDNA was RT–PCR amplified using primer pairs (forward primer - 5' GG GGT ACC ATG GAA TAT CAA CTA AGA GAA ATT 3' and reverse primer - 5' AAA CCT AGG GTT TTT TTC CAA TTT GCT CCT 3') and cloned into pARL (C terminus) vector using *Kpn*I/*Avr*II sites. Site-directed mutagenesis was performed to mutate S37 into A37 [using following primers: 5' TCA AAT AGT AAT GCC CAA ATT ACC GAA 3' and 5' TTC GGT AAT TTG GGC ATT ACT ATT TGA 3'], which was confirmed by sequencing and subsequently cloned into *Kpn*I/*Avr*II sites of pARL vector. For transfection, 100 μg circular plasmid DNA was used for electroporation and parasites were selected at 10 nM WR99210.

Plasmodium falciparum cultures and growth rate assays

Plasmodium falciparum 3D7 or PfCDPK7-KO (Kumar *et al*, 2014) parasites were cultured in complete RPMI 1640 medium with 0.3% albumax and gassed with 5% CO_2, 3% O_2, and 92% N_2 at 37°C. Synchronization of parasites was achieved by treatment with 5% sorbitol as described previously (Lambros & Vanderberg, 1979). PfCDPK7-KO parasites were maintained under 2.5 μg/ml blasticidine. 3D7 and PfCDPK7-KO were synchronized 2–3 times and ring-stage parasites were cultured in the presence or absence of 200 μM choline in the medium. For microscopic evaluation, Giemsa stained thin blood smears were prepared periodically and the parasitemia was determined. For quantitation by FACS, a previously described method was used with minor modifications (Theron *et al*, 2010). Similar protocol was followed for the growth comparison of parasites overexpressing EK-GFP or its S37A mutant, which were maintained under 10 nM WR99210.

For determining number of merozoites in schizonts, synchronized parasites were allowed to mature to schizont stage and 10 μM E64 was added. After 6 h, thin blood smears were made and stained with Giemsa. The number of merozoites per schizonts was counted while visualizing the smears under a light microscope.

Real-time PCR

For PfPMT qRT–PCR, schizont stage parasites were harvested and total RNA isolation was carried out using RNAeasy mini kit (Qiagen)

following manufacturer's instructions. 1 μg RNA was used for cDNA synthesis using random hexamers (SO142, Thermo Scientific), and qRT–PCR was performed in Real-Time Cycler (Eppendorf) using Dynamo Color Flash SYBR Green PCR Master Mix (F-416L, Thermo Scientific) and PfPMT-specific primers. 18S rRNA served as an internal control.

Immunofluorescence assays

The parasites were incubated with indicated primary antibodies at 4°C, washed with PBS, and incubated with Alexa Fluor 488 or 594 (488/594)-labeled secondary antibodies (Invitrogen) at room temperature. Following washing, mounting medium containing 4,6′-diamidino-2-phenylindole (DAPI) was used to stain the nucleus. The stained parasites were visualized using Axio Imager Z1 microscope or LSM700 confocal microscope (Carl Zeiss). Z stacking during image acquisition and processing of images was done using AxioVision 4.8.2 software. Z-stacks that best represented the immunolocalization were used for illustrations in the figures. Adobe Photoshop software was also used for preparing images for figures.

Western blotting

3D7 or other transgenic parasite lines were left untreated or treated with PI4K inhibitors as described in figure legends. Parasites pellets were used for preparing protein lysates and processed for Western blotting using various primary/secondary antibodies using standard procedures with the help of Pierce West Dura/Pico/Femto ECL reagent.

Lipid analysis and mass spectrometry-based lipidomic analyses

Plasmodium falciparum intraerythrocyte parasites (2×10^7 cell equivalents, equal loading for each sample) were harvested as described above for proteomics studies. Lipidomic analysis was carried out as described previously (Bansal *et al*, 2021). Briefly, lipids were extracted by a chloroform:methanol extraction, 1:2 (v/v), followed by chloroform: methanol extraction, 2:1 (v/v) and the organic phase was separated by adding 0.1% KCl, dried under N_2 flux and was dissolved in 1-butanol. For the total fatty acid analysis, an aliquot of the lipid extract was derivatized on-line using Meth-PrepII (Alltech) and the resulting FA methyl esters were analyzed by GC-MS as previously described (MacRae *et al*, 2012). For the quantification of each lipid, total lipid was separated by 2D HPTLC using first chloroform/methanol/28% NH_4OH, 60:35:8 (v/v/v) followed by 50:20:10:13:5 (v/v/v/v/v) for the 2nd dimension (Tanaka *et al*, 2012). Each lipid spot was extracted for quantification of fatty acids by gas chromatography–mass spectrometry (Agilent 5977A-7890B) after methanolysis (MacRae *et al*, 2012). Fatty acid methyl esters were identified by their mass spectrum and retention time and quantified by Mass Hunter Quantification Software (Agilent) using the calibration curve for fatty acid methyl esters standards mix (Sigma CRM47885). Subsequently, content of each lipid was normalized with respect to parasite cell number and a C21:0 internal standard (Avanti Polar lipids). All analyses were performed in triplicate or more ($n = 3$). P values of ≤ 0.05 from statistical analyses (t-tests) obtained from GraphPad software analysis were considered statistically significant.

Labeling of phospholipids (PLs) in *P. falciparum*

Synchronized 3D7 or PfCDPK7-KO, equal number of parasites were taken (as described above in proteomics section) and incubated at 37°C in the presence of 1.6 μCi/ml [^{14}C]-ethanolamine or 0.1 μCi/ml [^{14}C]-choline in complete RPMI–Albumax medium. After 12 h of incubation, the culture was harvested and parasites isolated with saponin lysis. Parasite pellet was washed twice with PBS. To assess the effect of PI4K inhibitor on PC/PE formation, 3D7 ring parasites were treated with either DMSO or MMV048 or UCT943 for 10–12 h prior to the addition of radiolabeled precursors. Subsequently, parasites were harvested after 12 h and processed as described above.

Total lipid isolation was performed using a previously described method (Bligh & Dyer, 1959). Lipids were resolved on TLC on silica gel-60 plates in chloroform, methanol, and NH_4OH (65:25:4, v/v/v) and visualized by phosphorimaging as described previously (Bansal *et al*, 2021). The fold change in radiolabeled PLs was determined after densitometry quantitation of radiolabeled bands/spots, which was done using ImageJ software.

Visualization of tubo-vesicular network (TVN)

BODIPY-TR Ceramide (Invitrogen, USA, Cat No. D7540) was used to stain TVN as described earlier (Elmendorf & Haldar, 1994). Briefly, BODIPY-TR-ceramide was prepared according to the manufacturer's protocol to obtain a 5 μM stock solution in 1× HBSS in sterilized condition. For live-cell imaging, cells from the parasite culture were removed, washed once in 1× HBSS and resuspended in an equal volume of 5 μM BODIPY-TR-ceramide solution and incubated for 30 min at 37°C. Stained infected RBCs were washed with 1× HBSS three times and examined by fluorescence microscopy; images were acquired and processed as described above.

FM4-64 uptake by *P. falciparum*

3D7 or PfCDPK7-KO-infected erythrocyte culture of mature trophozoite stages or either DMSO or PI4K inhibitor-treated 3D7 parasites were incubated with 16 μM FM4-64 (Invitrogen, USA, Cat No. F34653) for 30 min at 37°C in complete RPMI medium as described earlier (Lauer *et al*, 2000). Cells were washed twice, and the nucleus was stained using DAPI (1 μg/ml). ~1 million cells were counted in triplicate and monitored for mean fluorescence intensity of FM4-64 by using a FACS (BD Verse), and data were analyzed using Flow Jo software.

Generation of PMT antisera

For protein expression, PfPMT was cloned in *Bam*HI/*Hind*III site of pET28a vector. 6xHis-PfPMT protein was expressed in BL21(DE3)-RIL competent cells and purified using Ni-NTA column. Anti-PfPMT antisera were raised in rabbit against purified 6xHis-PfPMT protein.

Statistical analyses

The statistical analyses were performed using GraphPad PRISM. P-values of < 0.05 were considered as significant and n represents independent biological replicates.

Data availability

The mass spectrometry proteomics data have been deposited to the ProteomeXchange Consortium via the PRIDE partner repository with the dataset identifier Project accession: PXD025384 (https://www.ebi.ac.uk/pride/archive/projects/PXD025384).

Expanded View for this article is available online.

Acknowledgments
Studies were supported by grants BT/COE/34/SP15138/2015, and BT/PR7976/BRB/10/1223/2013 from Department of Biotechnology and SB/SO/BB/006/2014 from the Department of Science and Technology, India and funds from NII core. P.S. is a recipient of J.C. Bose Fellowship; P.B. and M.K. received Senior Research fellowship from CSIR. N.A. received Senior Research Fellowship from UGC. CYB and YYB were supported by Agence Nationale pour la Recherche, France (Grant# ANR-12-PDOC-0028 Project Apicolipid, and Grant# ANR-21-CE44-0010-01 Project ApicolipidAdapt), the Fondation pour la Recherche Médicale (FRM, Grant number EQU202102012700), Finovi programs (CNRS-INSERM-FinoviAtip-AvenirApicolipid projects), and the Laboratoire d' Excellence Parafrap, France (grant number ANR-11-LABX-0024), the Région Auvergne Rhone Alpes (IRICE grant, Project: GEMELI). The authors acknowledge Yenepoya (Deemed to be University) for access to mass spectrometry instrumentation facility. We also thank Ministry of Health and Family Welfare, Government of India for supporting with Orbitrap Fusion Tribrid instrument at NIMHANS-IOB Proteomic and Bioinformatics Laboratory. Authors would like to acknowledge Dr. Jeremy Burrows, MMV and Dr. Kelly Chibale for providing MMV390048 and UCT943, respectively.

Author contributions
PS, CYB, CD, and TSKP analyzed the data and wrote the manuscript. RM and AT, performed most experiments and were supported by PK and PB. MK, TSKP, and NA performed most of the proteomics experiments. YYB and CYB performed and analyzed all lipidomics datasets. Figures were prepared by authors involved in performing relevant experiments and were assembled by RM, AT, PS, YYB, CYB, and NA.

Conflict of interest
The authors declare that they have no conflict of interest.

References

Ahmed A, Gaadhe K, Sharma GP, Kumar N, Neculai M, Hui R, Mohanty D, Sharma P (2012) Novel insights into the regulation of malarial calcium-dependent protein kinase 1. *FASEB J* 26: 3212 – 3221

Alberge B, Gannoun-Zaki L, Bascunana C, Tran van Ba C, Vial H, Cerdan R (2009) Comparison of the cellular and biochemical properties of *Plasmodium falciparum* choline and ethanolamine kinases. *Biochem J* 425: 149 – 158

Balla T (2013) Phosphoinositides: tiny lipids with giant impact on cell regulation. *Physiol Rev* 93: 1019 – 1137

Bansal P, Antil N, Kumar M, Yamaryo-Botté Y, Rawat RS, Pinto S, Datta KK, Katris NJ, Botté CY, Prasad TSK *et al* (2021) Protein kinase TgCDPK7 regulates vesicular trafficking and phospholipid synthesis in Toxoplasma gondii. *PLoS Pathog* 17: e1009325

Billker O, Dechamps S, Tewari R, Wenig G, Franke-Fayard B, Brinkmann V (2004) Calcium and a calcium-dependent protein kinase regulate gamete formation and mosquito transmission in a malaria parasite. *Cell* 117: 503 – 514

Billker O, Lourido S, Sibley LD (2009) Calcium-dependent signaling and kinases in apicomplexan parasites. *Cell Host Microbe* 5: 612 – 622

Bligh EG, Dyer WJ (1959) A rapid method of total lipid extraction and purification. *Can J Biochem Physiol* 37: 911 – 917

Botte CY, Yamaryo-Botte Y, Rupasinghe TWT, Mullin KA, MacRae JI, Spurck TP, Kalanon M, Shears MJ, Coppel RL, Crellin PK *et al* (2013) Atypical lipid composition in the purified relict plastid (apicoplast) of malaria parasites. *Proc Natl Acad Sci U S A* 110: 7506 – 7511

Brancucci NMB, Gerdt JP, Wang CQ, De Niz M, Philip N, Adapa SR, Zhang M, Hitz E, Niederwieser I, Boltryk SD *et al* (2017) Lysophosphatidylcholine regulates sexual stage differentiation in the human malaria parasite *Plasmodium falciparum*. *Cell* 171: 1532 – 1544.e15

Brunschwig C, Lawrence N, Taylor D, Abay E, Njoroge M, Basarab GS, Le Manach C, Paquet T, Cabrera DG, Nchinda AT *et al* (2018) UCT943, a next-generation *Plasmodium falciparum* PI4K inhibitor preclinical candidate for the treatment of malaria. *Antimicrob Agents Chemother* 62: e00012-18

Cowman AF, Healer J, Marapana D, Marsh K (2016) Malaria: Biology and Disease. *Cell* 167: 610 – 624

Dechamps S, Maynadier M, Wein S, Gannoun-Zaki L, Marechal E, Vial HJ (2010a) Rodent and nonrodent malaria parasites differ in their phospholipid metabolic pathways. *J Lipid Res* 51: 81 – 96

Dechamps S, Shastri S, Wengelnik K, Vial HJ (2010b) Glycerophospholipid acquisition in Plasmodium – a puzzling assembly of biosynthetic pathways. *Int J Parasitol* 40: 1347 – 1365

Dvorin JD, Martyn DC, Patel SD, Grimley JS, Collins CR, Hopp CS, Bright AT, Westenberger S, Winzeler E, Blackman MJ *et al* (2010) A plant-like kinase in *Plasmodium falciparum* regulates parasite egress from erythrocytes. *Science* 328: 910 – 912

Elmendorf HG, Haldar K (1994) *Plasmodium falciparum* exports the Golgi marker sphingomyelin synthase into a tubovesicular network in the cytoplasm of mature erythrocytes. *J Cell Biol* 124: 449 – 462

Gaji RY, Checkley L, Reese ML, Ferdig MT, Arrizabalaga G (2014) Expression of the essential Kinase PfCDPK1 from *Plasmodium falciparum* in *Toxoplasma gondii* facilitates the discovery of novel antimalarial drugs. *Antimicrob Agents Chemother* 58: 2598 – 2607

Gulati S, Ekland E, Ruggles K, Chan R, Jayabalasingham B, Zhou B, Mantel P-Y, Lee M, Spottiswoode N, Coburn-Flynn O *et al* (2015) Profiling the essential nature of lipid metabolism in asexual blood and gametocyte stages of *Plasmodium falciparum*. *Cell Host Microbe* 18: 371 – 381

Kumar P, Tripathi A, Ranjan R, Halbert J, Gilberger T, Doerig C, Sharma P (2014) Regulation of *Plasmodium falciparum* development by calcium-dependent protein kinase 7 (PfCDPK7). *J Biol Chem* 289: 20386 – 20395

Kumar S, Kumar M, Ekka R, Dvorin JD, Paul AS, Madugundu AK, Gilberger T, Gowda H, Duraisingh MT, Keshava Prasad TS *et al* (2017) PfCDPK1 mediated signaling in erythrocytic stages of *Plasmodium falciparum*. *Nat Commun* 8: 63

Lambros C, Vanderberg JP (1979) Synchronization of *Plasmodium falciparum* erythrocytic stages in culture. *J Parasitol* 65: 418 – 420

Lauer SA, Rathod PK, Ghori N, Haldar K (1997) A membrane network for nutrient import in red cells infected with the malaria parasite. *Science* 276: 1122 – 1125

Lauer S, VanWye J, Harrison T, McManus H, Samuel BU, Hiller NL, Mohandas N, Haldar K (2000) Vacuolar uptake of host components, and a role for cholesterol and sphingomyelin in malarial infection. *EMBO J* 19: 3556 – 3564

Lemmon MA (2003) Phosphoinositide recognition domains. *Traffic* 4: 201

Lemmon MA, Ferguson KM (2001) Molecular determinants in pleckstrin homology domains that allow specific recognition of phosphoinositides. *Biochem Soc Trans* 29: 377 – 384

Lourido S, Shuman J, Zhang C, Shokat KM, Hui R, Sibley LD (2010) Calcium-dependent protein kinase 1 is an essential regulator of exocytosis in Toxoplasma. *Nature* 465: 359 – 362

MacRae JI, Sheiner L, Nahid A, Tonkin C, Striepen B, McConville MJ (2012) Mitochondrial metabolism of glucose and glutamine is required for intracellular growth of *Toxoplasma gondii*. *Cell Host Microbe* 12: 682 – 692

McCarthy JS, Donini C, Chalon S, Woodford J, Marquart L, Collins KA, Rozenberg FD, Fidock DA, Cherkaoui-Rbati MH, Gobeau N *et al* (2020) A phase 1, placebo controlled, randomised, single ascending dose study and a volunteer infection study to characterize the safety, pharmacokinetics and antimalarial activity of the Plasmodium phosphatidylinositol 4-kinase inhibitor MMV390048. *Clin Infect Dis* 71: e657 - e664

McNamara CW, Lee MCS, Lim CS, Lim SH, Roland J, Nagle A, Simon O, Yeung BKS, Chatterjee AK, McCormack SL *et al* (2013) Targeting Plasmodium PI(4) K to eliminate malaria. *Nature* 504: 248 – 253

Morlon-Guyot J, Berry L, Chen CT, Gubbels MJ, Lebrun M, Daher W (2014) The *Toxoplasma gondii* calcium-dependent protein kinase 7 is involved in early steps of parasite division and is crucial for parasite survival. *Cell Microbiol* 16: 95 – 114

Paquet T, Le Manach C, Cabrera DG, Younis Y, Henrich PP, Abraham TS, Lee MCS, Basak R, Ghidelli-Disse S, Lafuente-Monasterio MJ *et al* (2017) Antimalarial efficacy of MMV390048, an inhibitor of Plasmodium phosphatidylinositol 4-kinase. *Sci Transl Med* 9: eaad9735

Ramakrishnan S, Serricchio M, Striepen B, Butikofer P (2013) Lipid synthesis in protozoan parasites: a comparison between kinetoplastids and apicomplexans. *Prog Lipid Res* 52: 488 – 512

Reynolds JM, Takebe S, Choi JY, El Bissati K, Witola WH, Bobenchik AM, Hoch JC, Voelker DR, Mamoun CB (2008) Biochemical and genetic analysis of the phosphoethanolamine methyltransferase of the human malaria parasite *Plasmodium falciparum*. *J Biol Chem* 283: 7894 – 7900

Riglar DT, Richard D, Wilson DW, Boyle MJ, Dekiwadia C, Turnbull L, Angrisano F, Marapana DS, Rogers KL, Whitchurch CB *et al* (2011) Super-resolution dissection of coordinated events during malaria parasite invasion of the human erythrocyte. *Cell Host Microbe* 9: 9 – 20

Sebastian S, Brochet M, Collins MO, Schwach F, Jones ML, Goulding D, Rayner JC, Choudhary JS, Billker O (2012) A Plasmodium calcium-dependent protein kinase controls zygote development and transmission by translationally activating repressed mRNAs. *Cell Host Microbe* 12: 9 – 19

Solyakov L, Halbert J, Alam MM, Semblat J-P, Dorin-Semblat D, Reininger L, Bottrill AR, Mistry S, Abdi A, Fennell C *et al* (2011) Global kinomic and phospho-proteomic analyses of the human malaria parasite *Plasmodium falciparum*. *Nat Commun* 2: 565

Szklarczyk D, Franceschini A, Kuhn M, Simonovic M, Roth A, Minguez P, Doerks T, Stark M, Muller J, Bork P *et al* (2011) The STRING database in 2011: functional interaction networks of proteins, globally integrated and scored. *Nucleic Acids Res* 39: D561 – D568

Szklarczyk D, Franceschini A, Wyder S, Forslund K, Heller D, Huerta-Cepas J, Simonovic M, Roth A, Santos A, Tsafou KP *et al* (2015) STRING v10: protein-protein interaction networks, integrated over the tree of life. *Nucleic Acids Res* 43: D447 – 452

Tanaka T, Kassai A, Ohmoto M, Morito K, Kashiwada Y, Takaishi Y, Urikura M, Morishige J, Satouchi K, Tokumura A (2012) Quantification of phosphatidic acid in foodstuffs using a thin-layer-chromatography-imaging technique. *J Agric Food Chem* 60: 4156 – 4161

Tewari R, Straschil U, Bateman A, Bohme U, Cherevach I, Gong P, Pain A, Billker O (2010) The systematic functional analysis of Plasmodium protein kinases identifies essential regulators of mosquito transmission. *Cell Host Microbe* 8: 377 – 387

Theron M, Hesketh RL, Subramanian S, Rayner JC (2010) An adaptable two-color flow cytometric assay to quantitate the invasion of erythrocytes by *Plasmodium falciparum* parasites. *Cytometry A* 77: 1067 – 1074

Treeck M, Sanders JL, Gaji RY, LaFavers KA, Child MA, Arrizabalaga G, Elias JE, Boothroyd JC (2014) The calcium-dependent protein kinase 3 of toxoplasma influences basal calcium levels and functions beyond egress as revealed by quantitative phosphoproteome analysis. *PLoS Pathog* 10: e1004197

Witola WH, El Bissati K, Pessi G, Xie C, Roepe PD, Mamoun CB (2008) Disruption of the *Plasmodium falciparum* PfPMT gene results in a complete loss of phosphatidylcholine biosynthesis via the serine-decarboxylase-phosphoethanolamine-methyltransferase pathway and severe growth and survival defects. *J Biol Chem* 283: 27636 – 27643